

P11.1 THERMODYNAMIC CHARACTERIZATION OF SUPERCELL REAR-FLANK DOWNDRAFTS IN PROJECT ANSWERS 2003

Matthew L. Grzych, Bruce D. Lee and Catherine A. Finley

WindLogics, Inc.
Grand Rapids, Minnesota

John L. Schroeder
Texas Tech University
Lubbock, Texas

1. INTRODUCTION

Recently, much attention has been given to the rear-flank downdraft (RFD) and its association with tornadogenesis and tornadogenesis failure (Markowski et al. 2002, hereafter MSR2002; Markowski 2002). Research results revealed compelling evidence supporting the conclusion that RFD thermodynamic characteristics were a significant factor contributing to tornadogenesis and tornadogenesis failure. MSR2002 found that tornado likelihood, intensity, and longevity increased as the near-surface equivalent potential temperature (θ_e), virtual potential temperature (θ_v), and convective available potential energy (CAPE) increased and convective inhibition (CIN) decreased within the RFD.

Although the analyzed mobile mesonet dataset of RFD events presented by MSR2002 is considerable, it is not exhaustive given the variety of potential scenarios leading to tornadogenesis and the depth of the parameter space. Given this consideration, a primary objective of this research was to add to this observational RFD database through the analysis of the near-surface thermodynamic characteristics of 4 tornadic and 6 nontornadic RFDs. These datasets were collected during a field experiment conducted during May and June 2003. The following hypotheses, guided by the research of MSR2002, will be tested herein:

- RFDs characterized by small θ_e and θ_v deficits (as compared to inflow values), the presence of CAPE, and small CIN values are necessary for tornadogenesis
- RFDs characterized by large θ_e and θ_v deficits, the lack of CAPE, and significant CIN values are conditions conducive to tornadogenesis failure.

2. METHODS

Data for this work was collected during Project ANSWERS (Analysis of the Near-Surface Wind and Environment Along the Rear Flank of Supercells).

Corresponding author address: Matthew L. Grzych
WindLogics, Inc. – Itasca Technology Center
Grand Rapids, MN 55744
email: mattg@windlogics.com

Project ANSWERS was conducted on the Great Plains and in the Midwest during May and June of 2003 and consisted of 4 mobile mesonet stations (MM, Straka et al. 1996) collecting data every two seconds within tornadic and nontornadic supercell RFDs. Twelve second averaged data was used in most of the mesonet analysis. The mesonet dataset was bias checked/adjusted and quality controlled in a manner similar to MSR2002. The need for a flux gate compass (and its post-event quality control corrections) was removed by implementing field procedures that allowed the GPS to be used for vehicle direction at all times. Thermodynamic variables were calculated in a manner similar to MSR2002 with the exception of θ_v . Since most ANSWERS data was collected on storms at a significant distance from the nearest WSR-88D site, we had little confidence in estimating the liquid water mixing ratio (used for more accurately calculating θ_v) from the radar reflectivity (e.g., Rutledge and Hobbs 1984). The radar beam, at its lowest elevation angle of 0.5 degrees, samples the storm at a significant distance aloft (i.e., > 1 km for storms ~200 km from the radar). This resulted in the radar beam scanning echoes aloft that frequently were not reaching the ground (due to a strong updraft or evaporation) leading to unrepresentative surface radar reflectivity estimation.

CAPE and CIN were calculated utilizing the Rawinsonde Observation Program (RAOB). The atmospheric soundings analyzed were either obtained nearest to the storm event, both spatially and temporally, or most representative of the pre-storm environment. Due to the porous atmospheric sounding observational network, representing a storm's actual environment is difficult. Attempts have been made to alter the soundings by making them more representative of each event's pre-storm environment. Rapid Update Cycle model analysis data at 700, 850, and 925 mb (if applicable) were subjectively analyzed and placed into each sounding. Surface data within each sounding were represented by averaged MM fast temperature and dew point temperature observations for each RFD quadrant. Where surface elevations between the sounding site and the storm environment differed, surface elevations for the storm sounding were adjusted accordingly.

To obtain the perturbation equivalent potential temperature (θ_e') and perturbation virtual potential temperature (θ_v'), base states were calculated by linearly interpolating 10-minute average inflow

observations that were sporadically taken by the MM. This method has proven to be the most accurate in determining base states for Project ANSWERS data. Thermodynamic calculations derived from the nearest ASOS or AWOS data typically differed by several degrees from MM data. A possible reason for this difference is that ASOS and AWOS temperatures and dew points were rounded to the nearest whole number resulting in up to several degree errors in derived thermodynamic values. Another reason is that mesoscale thermodynamic gradients and fluctuations smaller than the observing network were present.

For each RFD event analyzed, a mesocyclone centroid was identified. When possible, the positions were found using WSR-88D velocity data. In cases when the mesocyclone was not detectable by radar, low-level mesocyclone positions were estimated using a triangulation technique, that was performed by analyzing photographs and video taken of tornadoes and wall clouds from multiple angles and positions. The tornadoes and wall clouds were assumed to be positioned in the low-level mesocyclone center. All analysis times were chosen to be within 10 minutes of tornadogenesis and tornadogenesis failure. Data points were plotted relative to WSR-88D radar data using a time-to-space conversion method described by MSR2002. The supercell radar echoes were assumed to be in steady state for 5 minutes, but allowed to translate horizontally. Essentially, this process put the observational MM data into the storm's positional frame of reference.

Due to logistical limitations, the area sampled in each RFD varied between events. Therefore, attempts have been made to qualify the density of observations in each event. The RFDs were broken down into four quadrants enclosed in a 4 km radius circle centered on the axis of rotation (Fig. 1, which was adopted from MSR2002). The line that separates quadrants I and IV from II and III passes through the low-level mesocyclone circulation center and is parallel to the neck of the hook echo. A 1 km buffer was then placed around each two-second data point for each event in an attempt to estimate the total percentage (to the nearest 10%) of each quadrant sampled within 1 km by the MM. Table 1 presents the percentages of each quadrant sampled for each event as well as each event's time, location, and characteristic. As may be seen in Table 1, quadrant III was well sampled in a large majority of events with poorer sampling for quadrants II and IV. Due to logistics and safety considerations, quadrant I was rarely sampled.

3. SELECTED EVENT ANALYSIS

A detailed examination of the RFDs analyzed reveals rather complex and intricate features associated with both tornadic and nontornadic events. In some cases analyzed, the RFDs were not thermodynamically and kinematically homogenous, but rather, the thermodynamic and/or kinematic fields varied dramatically over a distance of 1-2 km (see also P11.2, P11.3). Event 6 has been highlighted, which displays

the thermodynamic variability within an RFD over a small spatial scale (Fig. 2). KABR WSR-88D data at 0054 UTC was used as a reflectivity structural reference to overlay the time-to-space converted MM observations. At this time, the echo was approximately 200 km from the radar contributing to the distortion and horizontal placement relative to the MM. The supercell at analysis time was transitioning from classic to high-precipitation (HP) structural modes as hydrometeor concentration became greater behind and around the mesocyclone. At bottom left in Fig. 2, the photograph shows storm structure at approximate analysis time with the tail cloud, funnel cloud, and rain curtains visible. This has been classified as a tornadogenesis failure event as rapid low-level rotation and a funnel cloud evolved with no visual evidence of a tornadic circulation near the ground; however, DOW scans of the event at this approximate time indicated low-end tornadic strength winds near the surface (Josh Wurman, personal communication). Thus, in some cases, there is uncertainty how events such as this one get categorized. To underline the complex nature of the thermodynamic signal, the warmest θ_e conditions are actually just west and southwest of the low-level mesocyclone centroid. Perhaps this is the signal of a more undiluted RFD. The larger θ_e deficits are south of the mesocyclone where evaporation of hydrometeors falling into this air mass and deep mixing near the RFD boundary may be responsible for the cooler thermodynamic signal. At least in this case, if a mesonet only sampled that portion of the RFD 2-4 km south of the mesocyclone centroid, the potentially important "warm" RFD thermodynamic signal, would be missed.

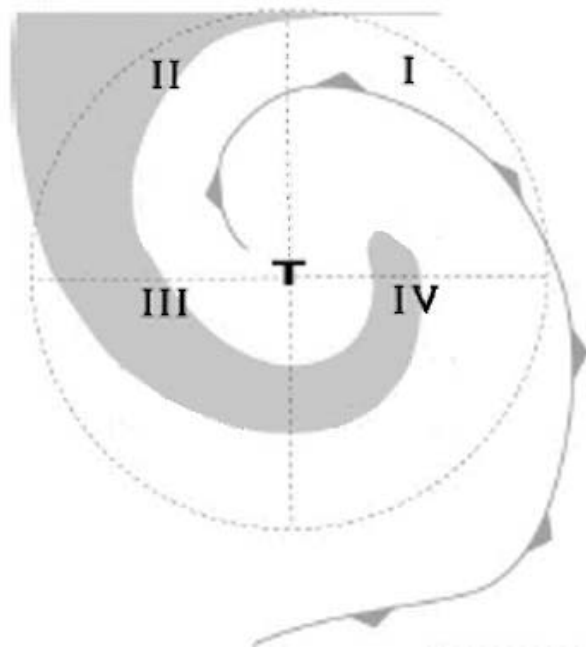


Figure 1. RFD quadrants. Adopted from MSR2002.

Table 1. RFD events in chronological order. Dates are relative to local time. Radar scan times (UTC) used for analysis are listed. Abbreviations for tornadic events are (TOR) and nontornadic events (NON).

Event	Type	Date	Location	Time	F-rating	% of Quadrant Sampled			
						I	II	III	IV
1	(TOR)	6/9/03	Springview, NE	2300	F0	20	40	30	0
2	(NON)	6/9/03	Newport, NE	2340		30	80	70	0
3	(TOR)	6/9/03	Oneill, NE	0054	F3	0	0	30	50
4	(NON)	6/11/03	Vivian, SD	2358		0	70	80	20
5	(NON)	6/11/03	Presho, SD	0034		0	0	80	80
6	(NON)	6/11/03	Kennebec, SD	0054		0	0	90	30
7	(NON)	6/24/03	Artesian, SD	2353		0	0	80	0
8	(NON)	6/24/03	Cavour, SD	0013		0	0	70	30
9	(TOR)	6/24/03	Manchester, SD	0042	F4	0	0	70	0
10	(TOR)	6/24/03	Spirit Lake, SD	0127	F1	0	10	80	0

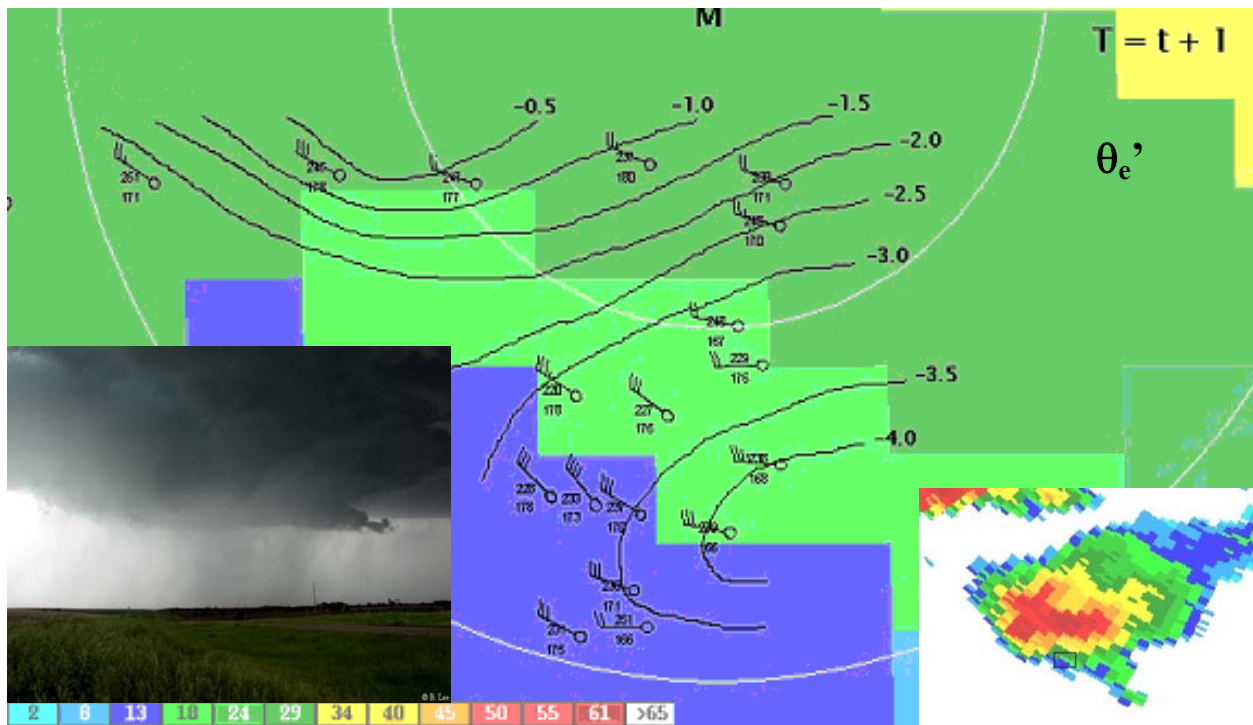


Figure 2. Subjective analysis of θ_e' at 0054 UTC for 12 June 2003 (11 June 2003 local time). Mobile mesonet station models include temperature top left in Celsius to the nearest tenth degree with decimal point excluded and dew point temperature bottom left in Celsius to the nearest tenth of a degree with the decimal point excluded. Data is plotted in the storm's frame of reference every 30 seconds. Tornadogenesis failure time (T) was 1 minute after analysis time (t). Photograph (bottom left) was taken at approximately 0055 UTC from the MM1 position looking north-northeast.

4. RESULTS

For each quadrant, θ_e' and θ_v' sample means (Table 2) were calculated from the mesonet data. The warmest average θ_e' air was found within quadrant III of Event 3's RFD, which was associated with a tornadic HP supercell that produced F3 damage. The coldest average θ_e' air was found within quadrant III of Event 8's

RFD, which was associated with a nontornadic RFD, although surprisingly, this event occurred two RFD cycles after an F3 tornado near Woonsocket, SD (see P11.2 for details on this case). A weak tornadic event (Event 10) was associated with the warmest average θ_v' air found, which was present within quadrant II with an average value 0.4 degrees warmer than the inflow air. The coldest average θ_v' air was found in quadrant II of

Event 2, which was a nontornadic RFD cycle that was associated with a tornadic supercell. Event 4 yields rather interesting results. As a nontornadic event, it ranked the second warmest average θ_e and third warmest θ_v , as compared to both tornadic and nontornadic events, suggesting that a warm RFD is not sufficient for tornadogenesis (see P11.2 for details on this case).

Values of CAPE and CIN were calculated for each event and quadrant (Table 3) by inserting the RFD quadrant's calculated sample mean temperature and dew point into each event's modified inflow sounding's lowest level. All RFDs observed by Project ANSWERS whether nontornadic, weak tornadic, or strong tornadic, contained a significant amount of CAPE. Nontornadic RFD CAPE values ranged from 1743 J/kg to 4364 J/kg. Tornadic RFD CAPE values ranged from 2346 J/kg to 4331 J/kg. Interestingly, the highest CAPE values were found within a nontornadic RFD (Event 7), which was associated with a previously tornadic supercell. CIN values for both tornadic and nontornadic RFDs ranged from -3 J kg^{-1} to -172 J kg^{-1} , with the greatest amount of CIN being found in quadrant II of a nontornadic RFD.

Average thermodynamic and stability parameters have been calculated for each RFD event's associated intensity level (nontornadic, weak tornadic, and strong tornadic) for each quadrant (Fig. 3). Due to logistical limitations and project objectives, certain quadrants were sampled more often than others. The general θ_e' trends are such that the greatest perturbations (coldest θ_e values) are found within the nontornadic RFDs and the smallest perturbations are found within strong tornadic RFDs. Trends in θ_v' are very similar to θ_e' trends where the nontornadic RFDs have the greatest θ_v perturbations, or coldest θ_v values, and weak tornadic and strong tornadic are warmer and warmest, respectively. CAPE trends follow a uniform increase from nontornadic through strong tornadic, while CIN trends are not quite as uniform with some variability in decreasing CIN values from nontornadic through strong tornadic.

Average thermodynamic and stability parameters were calculated for each category's entire RFD, including all quadrants (Table 4). Strong tornadic RFDs had an average θ_e' value 4.2 K warmer than nontornadic

Table 2. θ_e' and θ_v' sample means by quadrant and inflow θ_e and θ_v values used as a base state. (NON) represents a nontornadic event, (TOR) represents a tornadic event of F0 – F1 intensity, and (**TOR**) represents a tornadic event of F2 or greater intensity. A significant portion of the quadrant was not sampled if (*) is present.

Event	θ_e' (K) Quad. sample mean				Inflow θ_e (K)	θ_v' (K) Quad Sample Mean				Inflow θ_v (K)
	I	II	III	IV		I	II	III	IV	
1 (TOR)	-2.0	-2.6	-2.9	*	351.0	-1.1	-1.3	-1.3	*	310.5
2 (NON)	-4.6	-4.7	-3.9	*	351.6	-5.7	-5.6	-5.1	*	309.6
3 (TOR)	*	*	1.0	0.9	351.1	*	*	-0.1	-0.1	309.1
4 (NON)	*	-0.7	-0.3	-1.1	346.3	*	0.1	-0.7	-0.6	308.0
5 (NON)	*	*	-4.6	-4.7	346.2	*	*	-1.3	-1.3	307.7
6 (NON)	*	*	-2.4	-2.7	345.5	*	*	-2.9	-2.9	307.3
7 (NON)	*	*	-1.3	*	365.9	*	*	-0.4	*	308.2
8 (NON)	*	*	-13.1	-12.8	365.6	*	*	-2.5	-3.1	308.3
9 (TOR)	*	*	-2.7	*	365.1	*	*	-0.6	*	308.4
10 (TOR)	*	-1.4	-2.0	*	364.3	*	0.4	-0.5	*	308.6

Table 3. CAPE and CIN sample means by quadrant. Table designators as in Table 2.

Event	CAPE (J kg^{-1}) Sample Mean				CIN (J kg^{-1}) Sample Mean			
	I	II	III	IV	I	II	III	IV
1 (TOR)	2462	2428	2346	*	-141	-147	-150	*
2 (NON)	2547	2583	2679	*	-172	-170	-163	*
3 (TOR)	*	*	3397	3370	*	*	-88	-87
4 (NON)	*	2234	2333	2274	*	-42	-46	-44
5 (NON)	*	*	1743	1763	*	*	-83	-78
6 (NON)	*	*	1994	1972	*	*	-110	-76
7 (NON)	*	*	4364	*	*	*	-3	*
8 (NON)	*	*	2277	2793	*	*	-35	-39
9 (TOR)	*	*	4331	*	*	*	-8	*
10 (TOR)	*	4101	3998	*	*	-3	-14	*

RFDs, and weak tornadic RFDs had an average θ_e' value 2.2 K warmer than nontornadic RFDs. Strong tornadic RFDs had an average θ_v' value 2.9 K warmer than nontornadic events, and weak tornadic RFDs had an average θ_v' value 2.3 K warmer than nontornadic events. CAPE was 1187 J kg⁻¹ greater in RFDs associated with strong tornadic supercells than in RFDs associated with nontornadic supercells and 536 J kg⁻¹

greater in RFDs associated with weak tornadic supercells than in nontornadic supercells. CIN was 35 J kg⁻¹ less in RFDs associated with strong tornadic supercells than in RFDs associated with nontornadic supercells and 4 J kg⁻¹ less in RFDs associated with weak tornadic supercells than in nontornadic supercells.

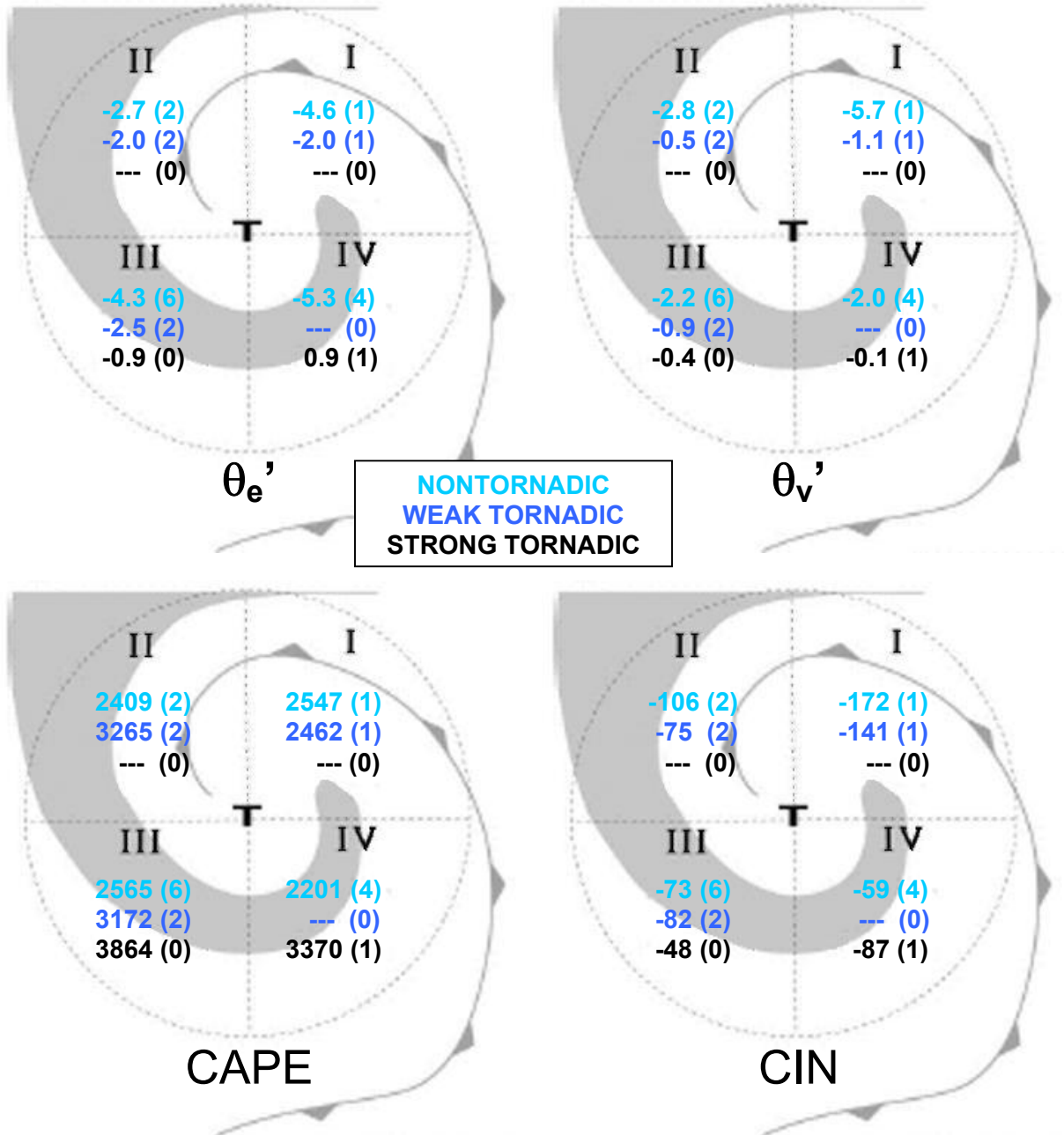


Figure 3. Average nontornadic, weak tornadic (< F2), and strong tornadic (\geq F2) RFD θ_v' , θ_e' , CAPE, and CIN by quadrant. Number of events analyzed given in parentheses.

Table 4. Average nontornadic, weak tornadic, and strong tornadic RFD θ_e' , θ_v' , CAPE, and CIN averaged over all quadrants.

	θ_e' (K)	θ_v' (K)	CAPE (J kg ⁻¹)	CIN (J kg ⁻¹)
Nontornadic	-4.2	-3.1	2430	-103
Tornadic < F2	-2.2	-0.8	2966	-99
Tornadic ≥ F2	0.0	-0.2	3617	-68

5. CONCLUSIONS

The current dataset of direct surface thermodynamic observations taken within supercell RFDs, although considerable in number, is not exhaustive to comprehensively represent the phenomena in the context of the tornadogenesis process. Thirty cases were examined in MSR2002, which resulted in several conclusions pertaining to RFD thermodynamics and its relationship to tornadogenesis and tornadogenesis failure. Data collected during Project ANSWERS presented an opportunity to test hypotheses based on conclusions from past work and provide additional datasets to the RFD observational database. Although only 10 cases are analyzed in this research, several provisional conclusions were developed based on the RFD analysis, which are as follows:

- On average, RFDs associated with tornadic supercells have surface θ_e and θ_v values equal to or slightly lower than storm inflow θ_e and θ_v values.
- RFDs associated with nontornadic supercells, on average, have θ_e and θ_v values 3-4 K colder than storm inflow θ_e and θ_v values. This suggests that nontornadic RFD air experiences some degree of evaporative cooling and/or mid-level air entrainment.
- The likelihood of tornadoes increases as RFD CAPE increases. Tornado strength increases as RFD CAPE increases.
- The likelihood and intensity of tornadoes increases as RFD CIN decreases.
- All supercell RFDs observed during Project ANSWERS, tornadic and nontornadic, had significant surface-based CAPE present. This may be highly dependent upon the fact that ambient CAPE values ranged from moderate to extreme during project operations. The significant RFD CAPE values may also be symptomatic of the difficulty in ascertaining a representative storm environment sounding.

- A thermodynamically “warm” RFD is not sufficient for tornadogenesis. Other factors most certainly play an important role in tornadogenesis as Events 4 and 7 were thermodynamically “warm”, but did not include tornadogenesis.

Even with the much smaller number of cases, results from the ANSWERS RFD analysis are consistent with a large portion of those presented in MSR2002. In general, they found that RFDs associated with tornadic supercells had θ_e' values 3 – 5 K warmer than RFDs associated with nontornadic supercells and RFDs associated with tornadic supercells had θ_v' values 3 – 4 K warmer than RFDs associated with nontornadic supercells. Their CAPE values were calculated from the level of free convection (LFC) up to 500 mb, which represents approximately 20% to 25% of the total CAPE. MSR2002 found that RFDs associated with tornadic supercells had 500 mb CAPE values of approximately 300 J kg⁻¹ (or 1200 J kg⁻¹ to 1500 J kg⁻¹ total CAPE) greater than RFDs associated with nontornadic supercells. They also found that nontornadic supercell RFDs contained 150 – 200 J kg⁻¹ more CIN than tornadic supercell RFDs. In the current study, tornadic supercell RFD θ_e' values were approximately 2 – 4 K warmer than nontornadic supercell RFD values and tornadic supercell RFD θ_v' values were approximately 2.5 – 3 K warmer than nontornadic supercell RFD values. Surface-based CAPE present in tornadic supercell RFDs ranged from being 500 – 1200 J kg⁻¹ greater than the surface-based CAPE found in nontornadic supercell RFDs. Nontornadic supercell RFD CIN values ranged from 5 - 35 J kg⁻¹ greater than tornadic supercell RFDs, notably smaller than the MSR2002 results. The consistency of the findings between the RFD thermodynamic analyses for the ANSWERS cases and those of MSR2002 are suggestive of a robustness in thermodynamic signal differentiating RFDs associated with tornadic events from those linked with non-tornadic events. A factor that may be important in future RFD mesonet data sampling lies in the quality of RFD thermodynamic signals obtained. As highlighted in section 3, the thermodynamic gradients can be quite strong with the potentially undilute signal of the RFD surge completely missed if mesonet data is gathered too far away. Likely, an even stronger thermodynamic signal would be captured if this more undilute RFD air was sampled.

6. ACKNOWLEDGEMENTS

This research was supported by the National Science Foundation under grants ATM-0105279 and ATM-0432408. The Department of Atmospheric Sciences at Texas Tech provided a mesonet station and support for the first author's participation in this project. The authors thank all Project ANSWERS 2003 participants for their contributions. Patrick Skinner, Erik Crosman, and Brian Guarente are recognized for their considerable efforts in managing software development and operational portions of the project.

7. REFERENCES

Markowski, P. M., 2002: Mobile mesonet observations on 3 May 1999. *Wea. Forecasting*, **17**, 430-444.

Markowski, P. M., J. M. Straka, and E. N. Rasmussen, 2002: Direct surface thermodynamic observations within the rear-flank downdrafts of nontornadic and tornadic supercells. *Mon. Wea. Rev.*, **130**, 1692-1721.

Rutledge, S. A., and P. V. Hobbs, 1984: The mesoscale and microscale structure and organization of clouds and precipitation in midlatitude cyclones. Part XII: A diagnostic modeling study of precipitation development in narrow cold-frontal rainbands. *J. Atmos. Sci.*, **41**, 2949-2972.

Straka, J. M., E. N. Rasmussen, and S. E. Fredrickson, 1996: A mobile mesonet for fine-scale meteorological observations. *J. Atmos. Oceanic Technol.*, **13**, 921-936.

